Ultrasensitive spectral trace detection of individual molecular components in an atmospheric binary mixture

Neil D. Weston, Palanikumaran Sakthivel, and Pritish Mukherjee

We present what is, to our knowledge, the first demonstration of the application of the laser homodyne interferometric technique to the quantitative identification of individual trace molecular constituents of a binary mixture in an ambient atmospheric background. Operation of the laser interferometric detection system to within a factor of 26 of the theoretical quantum noise limit, without extensive vibration isolation, is observed. We realize the spectral identification of SF_6 and CF_2Cl_2 mixed in various trace concentrations, without significant cross interference, using molecular spectral features overlapping the $10P$ CO_2 laser transitions.

Key words: Homodyne laser interferometry, trace detection, quantitative spectral identification, binary trace analysis, atmospheric trace monitoring.

1. Introduction

The detection of minute traces of contaminant gases in an ambient background is of great importance for civilian and military applications. In the civilian sector, atmospheric pollution monitoring has become a primary concern in the past decade. With increases in pollutants such as chlorofluorocarbons, hydrocarbons, and industrial waste [e.g., SO_2 and nitrogen oxides (NO_x)], it is important to have sensitive techniques that can detect these pollutants as well as measure their concentrations. Military applications require quantitative identification of chemical agents and toxins.

The use of lasers for molecular gas phase detection is based primarily on the absorption of energy. A desirable requirement for a suitable laser system is that the laser emission overlap as many absorption bands of different molecules as possible. An analysis of the applicability of different wavelength regimes is readily available in various publications.[1] Briefly, absorption in the microwave and the millimeter wavelength regions is problematic because of the existence of almost equal upper and lower state populations as a consequence of thermal population of the low-lying rotational states. The millimeter-to-far-IR region lacks a tunable laser source as well as a fixed frequency laser source with high power. In the near-IR, the existence of room-temperature diode lasers is attractive. However, molecular transitions in this region are typically weak as they are overtone transitions. The mid-IR source, therefore, emerges as the most desirable option for molecular excitation because of both the existence of strong molecular vibrational–rotational transitions and the availability of a number of tunable lasers.[2] The Pb salt diode laser can be tuned between 2 and 30 μm. The CO_2 and the CO lasers can provide high-power excitation in the 9–11-μm and 5–6-μm regions, respectively. The CO_2 laser is particularly suitable for atmospheric pollution monitoring as its emission range falls within the 8–14-μm atmospheric window.[1] Even though the Pb salt diode laser offers continuous tunability in contrast to the limitation of discrete line emissions from the CO_2 and CO lasers, its low output power (which is typically in the microwatt range) compared with the high power of IR gas lasers is a disadvantage. If the molecular absorption lacks exact coincidence with CO_2 and CO laser emissions, the spectral overlap may be enhanced by using suitable isotopic gas mixtures to increase the available spectrum of laser emission without compromising the power.

Various techniques have been used for the detection of molecules by using mid-IR laser excitation. Absorption and photothermal spectroscopy have

The authors are with the Department of Physics, Laboratory for Applied Laser Research, University of South Florida, Tampa, Florida 33620.

Received 1 July 1992.
0003-6935/93/060828-08$05.00/0.

yielded minimum absorption coefficients of the orders of 10^{-4} and 10^{-7} cm^{-1}, respectively. [3,4] FM spectroscopy has been demonstrated to be approximately 3 orders of magnitude more sensitive than absorption spectroscopy.[5] The most sensitive technique, until the advent of phase-fluctuation homodyne laser interferometry (HLI), had been photoacoustic spectroscopy, with the detectability of absorption coefficients as low as 10^{-10} cm^{-1}.[1,6,7] The pioneering work of Davis *et al.*[8–12] at the University of Maryland has demonstrated the possibility of sensitive detection by using the HLI technique for which a minimum detectable absorption coefficient (α_{min}) of 10^{-10} cm^{-1} was reported. In principle, improvements made to HLI can lower the measurable absorption coefficient to its theoretical limit of 10^{-11} cm^{-1}.

A key element in the use of HLI for the detection of trace species in the atmosphere is spectral recognition. This has been demonstrated for single-component hydrazines in a recent publication.[9] In this paper we describe the first application of the proven sensitivity of the homodyne laser interferometric technique, in conjunction with a tunable CO_2 laser, to spectroscopic identification and quantitative detection of individual trace components in a binary mixture in an ambient atmospheric background. In contrast to previous experiments that employed extensive vibration isolation and pure N_2 as a background gas to explore the theoretical limits of this technique in the laboratory, our current experiments were conducted under more realistic conditions, with ambient air as the atmospheric buffer for the trace constituents and without employing a complex vibration isolation scheme for the interferometer.

2. Experimental Details

The laser homodyne interferometer used for gas phase trace detection in our experiments is similar to that developed by Davis *et al.*[8,10] Early publications christened this technique phase-fluctuation optical heterodyne spectroscopy, but it has been more appropriately referred to as homodyne laser interferometry in a later publication.[11] Figure 1 shows a schematic representation of the interferometric detection system. The sample cell (10 cm long) containing the trace gas mixture is placed in one arm of a Mach–Zehnder single-frequency He–Ne laser interferometer. An amplitude-modulated, frequency-tunable, slow axial flow cw CO_2 laser is used as the excitation source and overlaps the interrogating He–Ne laser beam in the sample cell. The frequency-specific absorption of CO_2 laser power by the trace components, because of vibrational–translational relaxation, causes a thermally induced change in the density and consequently in the refractive index of the sample. The resulting signal that is due to the time-dependent change in the optical phase is detected by a Si photodiode at the output of the fractional-order interferometer. The signal causing the amplitude modulation of the CO_2 laser is used for phase-sensitive detection. Fringe stabilization between the interference maximum and minimum permits maximum responsivity and linearity for a small ac variation. The normalized HLI signal that is obtained as a function of the cw CO_2 laser frequency permits spectroscopic detection of trace constituents.

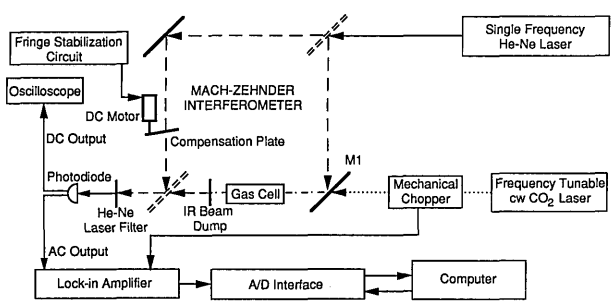

Fig. 1. Schematic diagram of the laser homodyne interferometric trace detection system. M1, mirror.

Experimentally, the spatial overlap of the CO_2 and the He–Ne laser beams was accomplished by using a Ge flat for mirror M1 in Fig. 1. This caused the He–Ne laser beam to be reflected while permitting the CO_2 laser beam to be overlapped subsequent to transmission. A shallow angle ($\sim 5°$) was used between the two beams to minimize overlap on the windows of the gas cell, thus reducing the possibility of spurious window signals. However, these signals did not, to first order, affect the accuracy of our measurements. The CO_2 beam was blocked by a glass plate (which is identified as the IR beam dump in Fig. 1) after passing through the gas cell. The dc output of the Si photodiode was used to bias the interferometer at the intermediate fringe position for linearity and maximum sensitivity, while the ac output at the chopping frequency of the CO_2 laser was detected by the lock-in amplifier as the HLI signal. This signal was stored on an IBM computer for subsequent data analysis. Fringe biasing for maximum sensitivity was achieved by using a dc motor to adjust the angle of a microscope slide and consequently control the relative path-length change. Neutral density filters, as necessary, were used to equalize the intensity of the He–Ne laser beam in the two arms of the interferometer for maximum fringe contrast. The interferometer arms were Invar stabilized to minimize thermal fluctuations in the path length. Acoustic vibrations were greatly reduced by enclosing the entire interferometer in an aluminum box. No further vibration isolation was used, in order to simulate realistic operational conditions.

The binary trace gas mixtures were prepared in unpurified ambient air by using a closed-cycle circulation system. Accurate volume calibrations, in conjunction with the method of successive dilutions, permitted the control of absolute concentrations of the relative trace constituents of the binary mixture, as required. The two trace constituents used in our experiments were SF_6 and CF_2Cl_2 (Freon-12). These two gases were chosen because of the presence of spectral features overlapping the $10P$ CO_2 laser transitions.

3. Theoretical Background

The theoretical basis for HLI has been well developed.[8,10,12] We review, briefly, the salient features of the technique as applicable to our experiments. The time-dependent phase fluctuation $\Delta\phi(t)$ of the single-frequency He–Ne laser beam that is due to the production of an expanding, cylindrically symmetric density wave following the heating caused by the absorption of IR laser radiation is given by

$$\Delta\phi(t) = \frac{2\pi l \Delta n(t)}{\lambda}, \tag{1}$$

where l is the absorber length, λ is the He–Ne laser wavelength, and $\Delta n(t)$ is the time-dependent refractive-index change of the sample. The electric field of the nonsampling beam of the interferometer can be represented in terms of its complex analytic signal as[10]

$$E_A(t) = A \exp[i(\omega t + \phi_A)], \tag{2}$$

where A is the amplitude of the electric field for the nonsampling beam and ω is the angular frequency, while the corresponding field for the probe arm, including the time-dependent phase fluctuation, is represented by[8,10]

$$E_B(t) = B \exp[i(\omega t + \phi_B + \Delta\phi(t)], \tag{3}$$

where B is the amplitude of the electric field for the probe arm. The He–Ne beams will have the same phase front curvature and can be aligned collinearly for optimum mixing at the photodetector. The interferometric intensity is

$$I = (E_A + E_B)(E_A + E_B)^*, \tag{4}$$

where $*$ denotes complex conjugation. For small $\Delta\phi(t)$ such that $\sin[\Delta\phi(t)] \approx \Delta\phi(t)$, Eq. (4) reduces to

$$I = A^2 + B^2 + 2AB[\cos(\phi_B - \phi_A) - \sin(\phi_B - \phi_A)\Delta\phi(t)], \tag{5}$$

so that the time-dependent portion of the intensity $I(t)$ is given by

$$I(t) = 2AB \sin(\phi_B - \phi_A)\Delta\phi(t). \tag{6}$$

The greatest sensitivity will be obtained when the phase difference between the two beams is adjusted so that

$$\phi_B - \phi_A = (2n - 1)(\pi/2), \tag{7}$$

where n is any integer. This condition is met when the interferometer path difference is adjusted so that the combined beams are midway between constructive interference and destructive interference. Under these conditions, Eq. (6) may be rewritten in the form

$$I(t) = 2AB\Delta\phi(t) \tag{8}$$

so that the time-dependent part of the detector signal $S(t) \propto 2AB\Delta\phi(t)$ is directly proportional to the induced phase fluctuation.

The output time-dependent voltage at the detector [when Eq. (1) is used] is given by

$$V = V_S \frac{2\pi l \Delta n(t)}{\lambda}, \tag{9}$$

where V_S is a system calibration constant.

For the general case in which $\Delta\phi(t) \ll 1$ does not hold, the complete form of Eq. (4), using Eqs. (2) and (3), leads to

$$S(t) = 2AB \sin(\phi_B - \phi_A)\sin[\Delta\phi(t)], \tag{10}$$

which, under condition (7), simplifies to

$$S(t) = 2AB \sin[\Delta\phi(t)], \tag{11}$$

thereby causing the output voltage at the detector to be represented as

$$V = V_S \sin \frac{2\pi l \Delta n(t)}{\lambda}. \tag{12}$$

The cw CO_2 laser that excites the gas in the sample cell is amplitude modulated by a mechanical chopper. The peak induced refractive-index change for a thin absorber ($\alpha l \ll 1$) at the chopping frequency ω_m is given by[12]

$$\Delta n \approx \frac{(n - 1)I_0\alpha}{2\rho\omega_m C_p T}, \tag{13}$$

where n is the index of refraction, α is the absorption coefficient, ρ and C_p are the density and the specific heat of the gas, respectively, T is the temperature, and I_0 is the unsaturated intensity of the CO_2 laser. The assumption is that the thermal conduction time τ_c is greater than ω_m^{-1}. For a thermal conduction velocity in air equal to 17 cm/s (see Ref. 9) and the average diameter of the He–Ne beam in the center of the cell equal to 1.40 mm, the experimental thermal relaxation time is approximately 8.24 ms. At the modulation frequency of 34 Hz (which was used in our experiments) $\tau_c > \omega_m^{-1}$, is, therefore, satisfied.

The minimum detectable refractive-index change for a signal-to-noise ratio of 1 is given by[8]

$$\Delta n_{\min} = \frac{c}{2\pi l \nu}\left(\frac{2h\nu\Delta f}{\eta P}\right)^{1/2}, \tag{14}$$

where P is the He–Ne laser power, η is the quantum efficiency of the detector, and Δf is the signal processing bandwidth. For $\eta = 0.5$, $l = 10$ cm, $P = 1$ mW, and $\Delta f = 1$ Hz, $\Delta n_{\min} \approx 3.57 \times 10^{-14}$.

The sensitivity for our HLI spectrometer can be described by the minimum detectable absorption

coefficient, which is represented by

$$\alpha_{\min} = \frac{2\omega_m \rho C_p T \Delta n_{\min}}{(n-1) I_0}. \quad (15)$$

When $\Delta n_{\min} \approx 3.57 \times 10^{-14}$, $I_0 = 1.60$ W/cm^2, $(n-1) = 2.9 \times 10^{-4}$, $T = 300$ K, $C_p = 1.006$ J g^{-1} °C^{-1}, $\omega_m = 2\pi$ (34 Hz), and $\rho = 1.189 \times 10^{-3}$ g/cm^3, Eq. (15) yields a value of approximately 1.18×10^{-8} cm^{-1} for $\alpha_{\min}$ for our system. For a higher CO_2 laser intensity (1 W focused to an ~0.5-mm spot size), this value may be decreased to $\sim 10^{-11}$ cm^{-1}.

4. Results and Discussion

A. Noise Measurements

There are two types of noise that are relevant in determining the theoretical detection limit for our experiments. One of them is the Johnson noise V_{jn} associated with thermal statistical fluctuations in the shunt resistance R of the photodiode, which is described by

$$V_{jn} = (4kTR\Delta f)^{1/2}. \quad (16)$$

For our system, V_{jn} was approximately 1.23×10^{-7} V for $T = 300$ K, $R = 909$ kΩ, and $\Delta f = 1$ Hz.

The other relevant noise source is the shot noise that is produced because of statistical fluctuations associated with the photocurrent and dark current of the detector as a result of the discreteness of the quantum of electric charge. The shot noise V_{sn} is described by

$$V_{sn} = (2qRV_{dc}\Delta f)^{1/2}, \quad (17)$$

where q is the electronic charge and V_{dc} is the signal voltage. In our system, $V_{sn} = 5.4 \times 10^{-7} (V_{dc})^{1/2}$. The combination of the signal-dependent shot noise and the constant Johnson noise was the theoretical quantum limit for signal detection.

In general, the noise signal may be represented as

$$V_n = A_n(t)\sin[\omega_t + \phi_n(t)], \quad (18)$$

where A_n is the time-dependent noise amplitude, ω is the modulation frequency, and $\phi_n(t)$ is the time-dependent phase. Noise measurements, therefore, pose the challenging problem of detecting a voltage that varies randomly in amplitude and phase.

We measured the noise voltage by detecting the ac component of the photodetector signal (within a 1-Hz bandwidth) with a lock-in amplifier tuned to the frequency of interest. Since the phase of the noise fluctuates randomly in time, the noise signal was observed for 60 s, and the maximum voltage was used as the measure of the noise voltage. Larger observation times yielded no significant changes in the maximum measured noise voltage. The lock-in detection frequency was swept through the desired range to obtain the noise spectrum. The dc output of the photodetector signal was simultaneously recorded and used as the signal for the corresponding signal-to-noise measurements.

A variety of operational conditions of the interferometer were assessed by means of the noise measurements. The factor $V_n/(V_{dc})^{1/2}$ may be used as a figure of merit that indicates a comparison of the experimental noise level with the theoretical quantum shot-noise limit [see Eq. (17)]. Single-beam noise measurements in the sampling and nonsampling arms of the interferometer yielded values ~1.2 times the quantum noise limit.

The noise limitations to the sensitivity of detection are anticipated, however, to be much more severe in the dual-beam operation of the interferometer, particularly in the maximum sensitivity intermediate interference mode. Even though an increase in the signal-to-noise ratio at higher frequencies was observed in the noise spectra, consistent with the trend expected of vibrationally induced noise, the thermal diffusion time of ~8 ms restricts the practical upper frequency limit for trace detection.

The low-frequency range suitable for interferometric operation was investigated vis-à-vis noise characteristics at a resolution of 1 Hz. The noise spectral data between 10 and 50 Hz are plotted in Fig. 2. The highest signal-to-noise level was observed at 34 Hz. The corresponding plot of $V_n/(V_{dc})^{1/2}$ yields a value of noise that is ~30 times the theoretical shot-noise limit. Based on the dual criteria of minimum noise and acceptable thermal diffusion, a modulation frequency of 34 Hz was used in all the subsequent data.

B. Single-Component Trace Detection

A small, deliberately introduced misalignment in the two He–Ne beams that recombine after exiting the interferometer may be used to generate a larger number of spatial interference fringes within the spot size of the laser beam at the output of the interferometer. A study to analyze the effect of the number of fringes on the achievable sensitivity was performed by using the experimental arrangement depicted in Fig. 3. After exiting the interferometer, the recombined He–Ne laser beams were incident upon a variable aperture. The portion of the interference

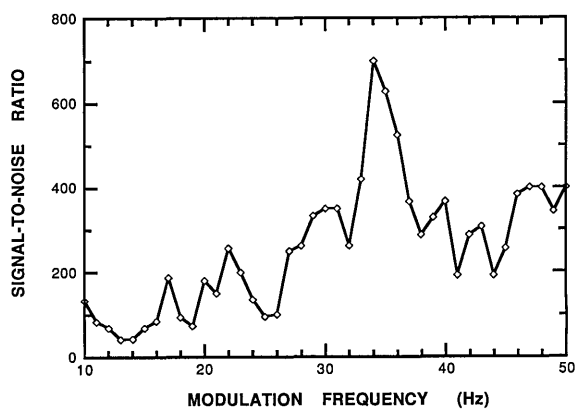

Fig. 2. Low-frequency noise characteristics for dual-beam interferometer operation in the intermediate mode.

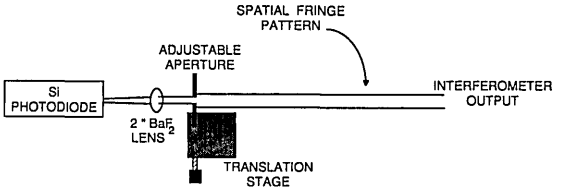

Fig. 3. Optical arrangement for variable aperturing of a section of the spatial fringe pattern.

fringe passing through the aperture was focused onto the Si photodiode with a 2-in. (5.08-cm) BaF_2 lens. This prevented any possible loss as a result of diffraction caused by the slit. The aperture of the slit may be adjusted to achieve any desired contrast ratio (ratio of the intensity at the interference maximum to the interference minimum), which is essentially a measure of the slope of the intensity in the spatial interference pattern. A large contrast ratio implies a larger HLI signal for the same phase fluctuation, if the He–Ne laser power remains constant.

In a practical application, the contrast ratio is enhanced by decreasing the slit width, which also decreases the laser power that is incident upon the detector. An optimum value exists at which the trade-off between the laser power and the contrast ratio is balanced. This is illustrated in Fig. 4, in which the HLI signal [for 25-parts-in-10^6 (ppm) SF_6 excited by the $10P(14)$ CO_2 laser transition] is shown as a function of the contrast ratio (adjusted by a variable slit width). The different curves correspond to a variable number of interference fringes across the laser spot. Depending on the number of fringes, the highest signal was achieved at a contrast ratio of 6–10. Above this value, the decrease in incident laser power on the photodetector reduces the signal, while below it the low contrast ratio leads to decreased sensitivity. The use of two fringes across the laser beam was observed to optimize the signal. This arrangement was accepted, therefore, as the system of choice for subsequent experiments.

The ν_3 fundamental mode of SF_6 was resonantly excited by using the $10P(14)$ CO_2 laser transition to study the variation of the HLI signal as a function of CO_2 laser power. A concentration of 9800 ppm of SF_6 in ambient air was used for this experiment. The HLI signals obtained for different CO_2 laser intensities are plotted in Fig. 5. The plot indicates that the signal increases linearly at low laser intensities but begins to level off as the intensity increases further. The experimental data are numerically consistent with the behavior predicted by Eq. (12) and approximation (13) with $\sigma = 1.3 \times 10^{-17}$ cm^2, which is in agreement with the published value of σ in Ref. 13.

The detection sensitivity of our system was assessed by studying the variation of the HLI signal as a function of the trace concentrations of SF_6 and CF_2Cl_2. It must be emphasized that other than enclosure of the interferometer (including the cell) by an aluminum box, no other means were adopted to reduce acoustic noise. This was done to simulate natural operating conditions, in contrast to previous experimental work in which massive flotation tables were used for vibration isolation.[8,10] Mechanical vibrations shared by both arms of the interferometer are, of course, canceled out by the homodyne signal detection process.

Trace detection of SF_6 was studied at the peak of the ν_3 fundamental band by using a constant CO_2 laser intensity of 1.60 W/cm^2. Samples of various trace concentrations of SF_6 in ambient air were prepared by using the method of successive dilutions, and their corresponding HLI signals were recorded. Figure 6 is a plot of the HLI signal as a function of the trace SF_6 concentration. The log–log plot can be extrapolated to yield the detection sensitivity. In order to calculate the minimum detectable concentration of SF_6, we recorded the noise level by measuring the HLI signal with ambient air in the gas cell. This noise signal, therefore, includes the contribution of possible window signals as well as contributions that are due to contaminants in the ambient air. The measured noise level of ~ 25 μV permits a detectability of 15 parts in 10^9 (ppb) of SF_6. For $\sigma_{SF_6} = 1.3 \times 10^{-17}$ cm^2, this leads to a measurable Δn of 1.48×10^{-11} when approximation (13) is used. A comparison of this experimental result with theoretical predic-

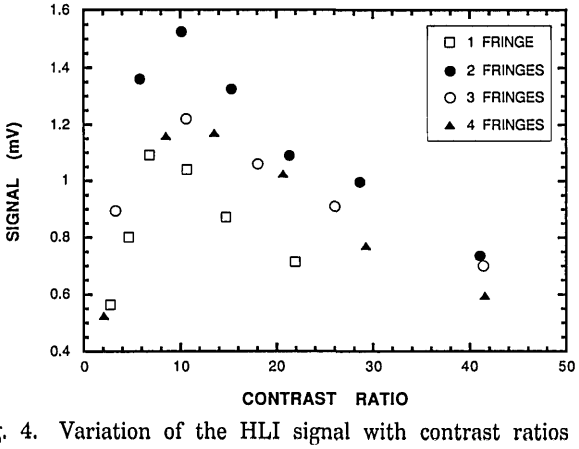

Fig. 4. Variation of the HLI signal with contrast ratios for different fringe patterns.

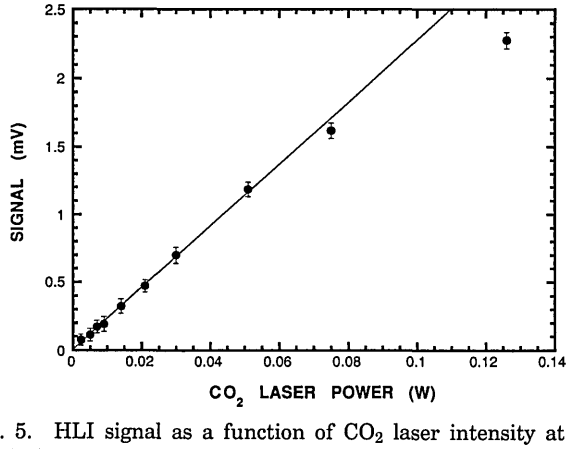

Fig. 5. HLI signal as a function of CO_2 laser intensity at the $10P(14)$ laser transition for 9800 ppm of SF_6 in ambient air. The solid line indicates a linear fit to the low-intensity data.

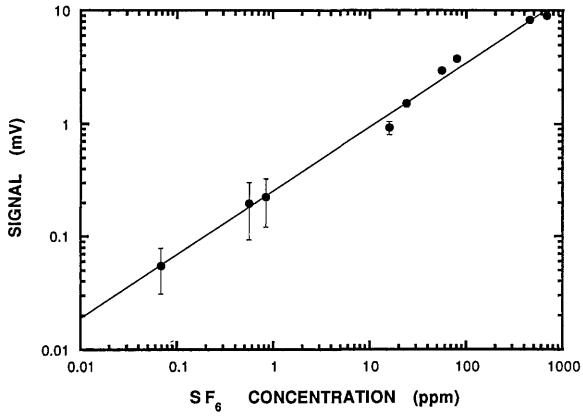

Fig. 6. SF_6 concentration dependence of the HLI signal at the $10P(14)$ CO_2 laser transition.

tion is possible by independently calculating Δn_{min}, using Eq. (14). For the measured He–Ne laser power of 4 μW that is incident upon the photodetector after the slit, Eq. (14) yields $\Delta n_{min} = 5.7 \times 10^{-13}$. The experimental result is, therefore, within a factor of 26 of the theoretical quantum noise limit.

A trace detection study was also conducted for CF_2Cl_2 (Freon-12) by using the absorption feature that is resonant with the $10P(32)$ CO_2 laser line. Figure 7 shows a log–log plot of the HLI signal versus the trace concentration of CF_2Cl_2. Extrapolation back to the noise level demonstrates a minimum detectable trace concentration of ~4 ppm. A numerical simulation of the experimental results by solving Eq. (12) and approximation (13), including CO_2 laser energy variations during propagation through the gas cell, yields a value of $\sigma = 8.7 \times 10^{-19}$ cm^2 for CF_2Cl_2 at the $10P(32)$ CO_2 laser transition, which is consistent with the corresponding small-signal value of σ obtained from absorption data published in Ref. 14.

The overall sensitivity of the trace detection system can be obtained from its minimum detectable absorption coefficient. For our system, the detection of an absorption coefficient of $\sim 1.2 \times 10^{-8}$ cm^{-1} for a 1-mW He–Ne laser power and a moderate CO_2 laser intensity of 1.6 W/cm^2 is possible. An extension to $\sim 10^{-11}$ cm^{-1} for a 1-W CO_2 laser focused to a spot size of 0.5 mm has been indicated. Despite the lack of extensive vibration isolation, operation of the HLI system to within a factor of 26 of the theoretical noise limit is demonstrated. Further improvement by the use of novel interferometric arrangements should be possible. Some possible improvements include, for example, enhancement of the HLI signal by introducing longer path lengths in a multipass arranagement and further reduction of acoustic noise by using an evacuated interferometer.

C. Spectral Detection of Binary Trace Components

Practical applications of the HLI technique for trace detection depend on the capability of identifying individual trace species in a complex mixture. This should be possible by means of spectral recognition, as each molecule has a specific absorption band or signature that distinguishes it from other molecules. For spectroscopic trace detection, high spectral resolution or spectral separation of key identifying features is the main concern for proper identification. The HLI technique was used to obtain the absorption spectrum of trace molecules by tuning through the suitable frequency range of the amplitude modulated cw CO_2 laser and recording the corresponding HLI signal at each frequency.

The HLI spectrum of SF_6 was obtained by using the ν_3 band absorption, which was chosen as it overlaps the $10P$ CO_2 laser transitions. A trace concentration of 16 ppm of SF_6 in ambient air was used for the experiment. The HLI signal and the incident CO_2 laser power were recorded for each CO_2 laser transition. This data was used to normalize the HLI signal with respect to variations in the laser power at different CO_2 laser frequencies. The normalized HLI spectrum for SF_6 is shown in Fig. 8. The HLI spectrum coincides with the expected absorption profile ranging from the $10P(6)$ to the $10P(32)$ CO_2 laser transitions with a peak absorption at ~949.5 cm^{-1}. The observed spectral asymmetry is consistent with previously reported absorption spectra for SF_6 obtained at a 2-cm^{-1} spectral resolution.[15]

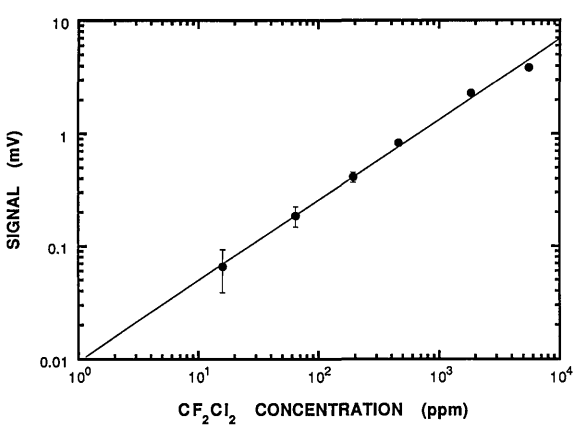

Fig. 7. CF_2Cl_2 concentration dependence of the HLI signal at the $10P(32)$ CO_2 laser transition.

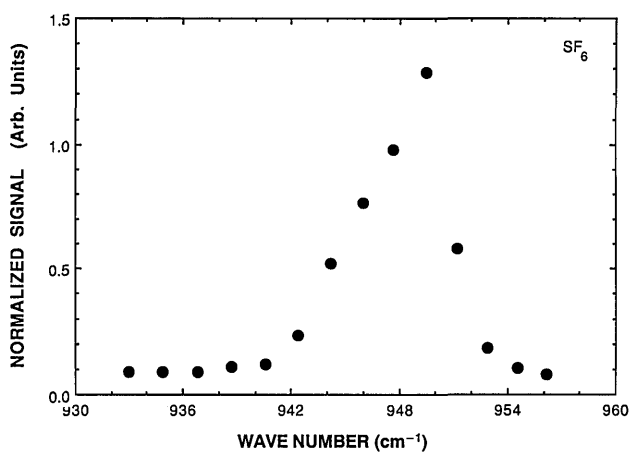

Fig. 8. Normalized HLI spectrum for 16 ppm of SF_6 in an ambient atmospheric background.

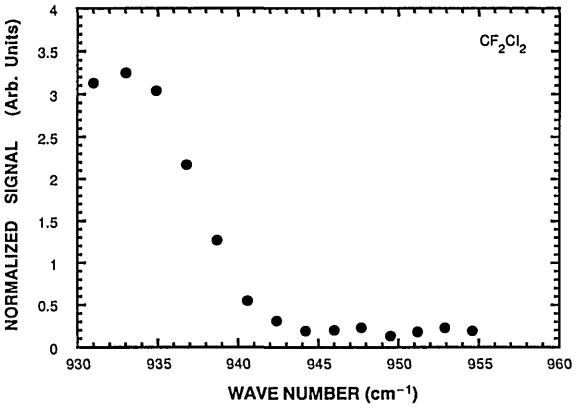

Fig. 9. Normalized HLI spectrum for 454 ppm of CF_2Cl_2 in an ambient atmospheric background.

The resonant feature in the absorption spectrum of CF_2Cl_2 that overlaps the $10P$ CO_2 laser branch was used to obtain its HLI spectrum. The normalized spectrum at a CF_2Cl_2 concentration of 454 ppm in ambient air is shown in Fig. 9. The peak of the spectral feature occurs at the $10P(32)$ CO_2 laser transition.

The ability to distinguish differing trace concentrations of SF_6 and CF_2Cl_2 in a binary mixture was studied by maintaining the SF_6 concentration at 16 ppm (which is consistent with the spectrum recorded in Fig. 8), while the CF_2Cl_2 concentration was deliberately enhanced to 13,000 ppm. The resultant HLI spectrum over the $10P$ CO_2 laser transitions is shown in Fig. 10. The peak at $10P(14)$ corresponds to the absorption that is due to SF_6. The normalized signal at the $10P(14)$ line is in good agreement with the trace detection data (Fig. 6) for the same concentration. The location of the peak also matches the spectral peak from the absorption spectrum of SF_6 in ambient air. The asymmetric features are similar to those of Fig. 8. The CF_2Cl_2 band dominates between 929 and 944 cm^{-1} and agrees with the profile illustrated in Fig. 9. The $10P(32)$ peak signal corresponds to that obtained in Fig. 7 for a concentration

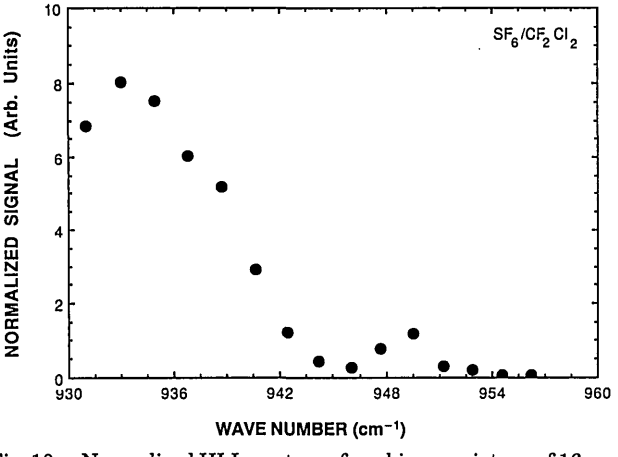

Fig. 10. Normalized HLI spectrum for a binary mixture of 16 ppm of SF_6 and 13,000 ppm of CF_2Cl_2 in an ambient atmospheric background.

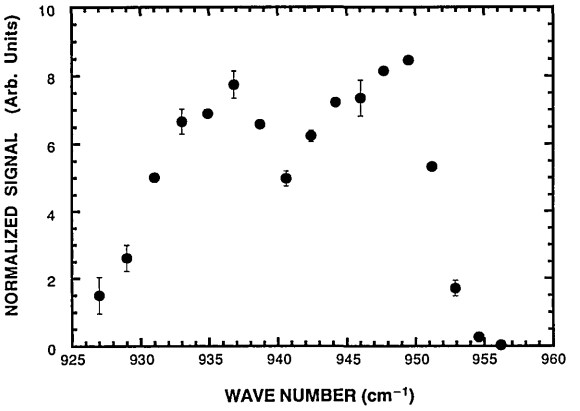

Fig. 11. Normalized HLI spectrum for a binary mixture of 454 ppm of SF_6 and 13,000 ppm of CF_2Cl_2 in an ambient atmospheric background.

of 13,000 ppm. The capability of resolving a much smaller spectral signal from SF_6 against the large-background CF_2Cl_2 absorption is evident. Figure 11 is another spectral profile of SF_6 (454 ppm) and CF_2Cl_2 (13,000 ppm). Again, the peak absorptions that correspond to their individual profiles are obtained. However, distortions at intermediate frequencies caused by overlapping of the absorption lines is evident.

The individual peak HLI signals at 949 cm^{-1} (for SF_6) and 933 cm^{-1} (for CF_2Cl_2) were used to study systematically the effects of a variable ratio of the two constituents in a binary mixture. For these experiments, the SF_6 concentration was held invariant at 16 ppm while the CF_2Cl_2 concentration was altered in the binary mixture in several steps from 15 to 6000 ppm. The resultant normalized ratios of HLI signals for CF_2Cl_2 and SF_6 are shown in Fig. 12 as a function of their relative concentrations. An independent verification of the lack of interference between the two peak signals is possible by comparing the experimental data in Fig. 12 with those expected

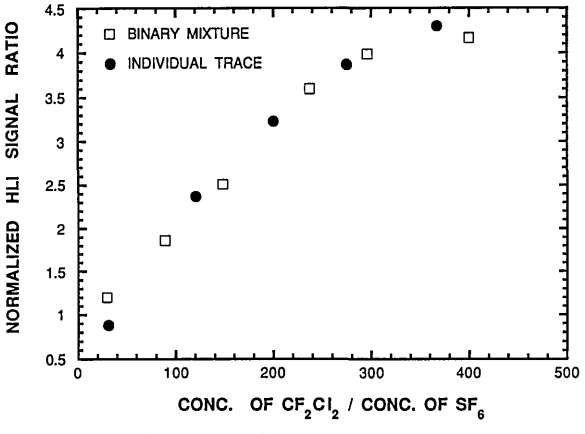

Fig. 12. Ratio of HLI signals versus relative concentrations of CF_2Cl_2 and SF_6 in the binary trace mixture in ambient air. The open squares show values based on binary spectral detection, while the filled circles indicate ratios obtained from individual trace detections, for comparison.

on the basis of the individual trace detection signals reported in Figs. 5 and 6. The data obtained from the binary mixture is plotted along with expected results from the individual trace signals in Fig. 12. The excellent agreement indicates the capacity to isolate the individual peak signals for SF_6 and CF_2Cl_2 in a binary mixture without significant interference.

5. Conclusion

In summary, the spectroscopic capabilities and sensitivity of the homodyne laser interferometric technique were used to demonstrate what is, to our knowledge, the first application to identification and quantification of individual components in a binary trace mixture in an ambient atmospheric background. Significantly, our HLI system detected trace concentrations as low as 16 ppb of SF_6 and 4 ppm of CF_2Cl_2, which represents an operation of a factor of 26 above the theoretical quantum noise limit without extensive vibration isolation. Improvements in the interferometer, the detection system, and the reduction of noise should further lower the detectable concentration under realistic background conditions. The spectral identification of SF_6 and CF_2Cl_2, mixed at various trace concentrations, was easily possible without significant cross interference. Our investigation indicates that the HLI system can be used in the tunable mode as a means of identifying individual trace components in a more complex gas mixture by means of spectral recognition. Experiments are currently in progress with spectrally interfering multicomponent trace mixtures, in which the additional challenge of spectral deconvolution will be addressed.

Any correspondence should be addressed to P. Mukherjee.

References and Notes

1. P. L. Meyer and M. W. Sigrist, "Atmospheric pollution monitoring using CO_2 laser photoacoustic spectroscopy and other techniques," Rev. Sci. Instrum. **61,** 1779–1807 (1990), and references contained therein.
2. O. Svelto, *Principles of Lasers,* 3rd ed. (Plenum, New York, 1989), Chap. 6, p. 374.
3. N. J. Novichi and J. M. Harris, "Differential thermal lens calorimetry," Anal. Chem. **52,** 2338–2342 (1980).
4. K. H. Fung and H.-B. Lin, "Trace gas detection by laser intracavity photothermal spectroscopy," Appl. Opt. **25,** 749–752 (1986).
5. D. E. Cooper and T. F. Gallagher, "Frequency modulated spectroscopy with a CO_2 laser: results and implications for ultrasensitive point monitoring of the atmosphere," Appl. Opt. **24,** 710–716 (1985).
6. C. K. N. Patel and R. J. Kerl, "A new optoacoustic cell with improved performance," Appl. Phys. Lett. **30,** 578–579 (1977).
7. P. Hess and J. Pelzl, eds., *Photoacoustic and Photothermal Phenomena* (Springer-Verlag, Berlin, 1988), Part III, pp. 114–149.
8. C. C. Davis, "Trace detection in gases using phase fluctuation optical heterodyne spectroscopy," Appl. Phys. Lett. **36,** 515–518 (1980).
9. D. L. Mazzoni and C. C. Davis, "Trace detection of hydrazines by optical homodyne interferometry," Appl. Opt. **30,** 756–764 (1991).
10. C. C. Davis and S. J. Petuchowski, "Phase fluctuation optical heterodyne spectroscopy of gases," Appl. Opt. **20,** 2539–2554 (1981).
11. T. J. F. Carr-Brion, D. Mazzoni, A. Gungor, and C. C. Davis, "Improved system for trace gas detection using homodyne laser interferometry," in *Conference on Lasers and Electro-Optics,* Vol. 7 of 1988 OSA Technical Digest Series (Optical Society of America, Washington, D.C., 1988), pp. 78–80.
12. A. J. Campillo, H. Lin, C. J. Dodge, and C. C. Davis, "Stark-effect-modulated phase-fluctuation optical heterodyne interferometer for trace gas analysis," Opt. Lett. **5,** 424–426 (1980).
13. A. V. Nowak and J. L. Lyman, "The temperature-dependent absorption spectrum of the ν_3 band of SF_6 at 10.6 μm," Quantum Spectrosc. Radiat. Transfer **15,** 945–961 (1975).
14. CCl_2F_2 Spectrum no. 6837K (Sadtler Research Laboratories, Inc., Allied Chemical Corp., Morristown, N.J.).
15. H. Kildal and T. F. Deutsch, "Infrared third-harmonic generation in molecular gases," IEEE J. Quantum Electron. **12,** 429–435 (1976).